Feasibility study of resistance spot welding of dissimilar Al/Mg combinations with Ni based interlayers

P. Penner*[1], L. Liu[2], A. Gerlich[1] and Y. Zhou[1]

Microstructure and mechanical properties of the dissimilar aluminium–magnesium resistance spot welds made with gold coated and bare nickel interlayers are investigated. Welds were made with different welding currents in a range from 16 to 24 kA and fixed welding time of five cycles. No joints were achieved with a bare nickel interlayer; after welding, specimens were separated without applying any force. Addition of gold coating on nickel surface greatly contributed to the metallurgical bonding at the interfaces and welds easily met requirements of AWS D17·2 standard. Average lap shear strength reached 90% of similar AZ-31B spot weld strength. Fusion nugget size, interfacial microstructure and fracture surface morphology of the welds were analysed.

Keywords: Magnesium, Aluminium, Nickel, Interlayer, Dissimilar, Resistance spot welding

Introduction

The automotive industry is continually struggling to improve fuel efficiency by employing lightweight materials such as aluminium and magnesium alloys, since reducing vehicle weight can greatly lower fuel consumption. It was reported that 100 kg of reduced vehicle weight saves ~0·3 L of fuel per 100 km.[1] Although some aluminium based frame structures have been produced, utilisation of these alloys has generally been incremental and resulted in designs which employ multiple materials, which often need to be joined in dissimilar combinations.

Since aluminium and magnesium alloys can both be potentially used in the same structure, the problem of joining these two materials must be addressed. Numerous studies regarding dissimilar joining of aluminium to magnesium by different techniques can be found in the literature. The common problem with all fusion based dissimilar metal joining techniques of aluminium to magnesium is the formation of hard and brittle intermetallic compounds.[2–5] Solid state processes which involve comparatively low temperatures such as diffusion bonding,[6,7] friction stir welding (FSW),[8–10] friction stir spot welding (FSSW)[11,12] and ultrasonic spot welding can achieve relatively high strength;[13,14] however, even in this case, the formation of brittle Al–Mg intermetallic compounds cannot be completely avoided.

To mitigate the formation of undesirable intermetallics, some work has been carried out to explore the effect of different interlayers on the properties of aluminium–magnesium joints. A variety of interlayers such as zinc,[15] cerium,[16] silver,[17] tin,[18] titanium,[19] copper,[20] nickel and others were incorporated with different solid and non-solid state welding processes.[21,22] In general, employing interlayers reduced fraction of Al–Mg intermetallics and improved mechanical properties of the joints. It also was noted that better results were achieved when interaction between aluminium and magnesium was completely suppressed. For example, during diffusion bonding of aluminium to magnesium with silver foil interlayer,[17] better results were achieved with medium temperatures when diffusion was not intense enough to let magnesium and aluminium interact. With increasing temperature, diffusion of aluminium and magnesium atoms became more intense and formation of Al–Mg intermetallics was observed.

Resistance spot welding (RSW) of aluminium to magnesium is particularly interesting since it is the predominant joining technique in the automotive industry. Nevertheless, only one detailed study on RSW of aluminium to magnesium is available in the literature.[4] The strength of the welds achieved in this study was negatively influenced by the formation of brittle intermetallic compounds. In addition, this study considered commercially pure aluminium, which inevitably would result in low strength joints due to fracture propagation through the soft base metal as well. A suitable technology for achieving high strength aluminium–magnesium welds by RSW has yet to be developed.

Considering information available in the literature, employing an interlayer during welding of aluminium to magnesium might be a feasible approach to eliminate intermetallics and improve mechanical properties of the joints during RSW. As was noted, it is better to completely avoid interaction between aluminium and magnesium. Employing an interlayer with a high melting point, which will remain intact during the RSW, should entirely prevent

[1]Department of Mechanical and Mechatronics Engineering, University of Waterloo, Waterloo, Ont N2L 3G1, Canada
[2]Department of Mechanical Engineering, Tsinghua University, Beijing 100084, China

*Corresponding author, email ppenner@uwaterloo.ca

Published by Maney on behalf of the Institute
Received 7 January 2013; accepted 12 April 2013
DOI 10.1179/1362171813Y.0000000129

the formation of Al–Mg intermetallics. Nickel based foils are strong candidates to the interlayers. The high melting point of nickel (1455°C) compared to magnesium (650°C) and aluminium (660·42°C) will prevent mixing of aluminium and magnesium during RSW. In addition, Al–Ni and Mg–Ni intermetallics are less brittle and therefore more preferable than Al–Mg intermetallics.[22,23] Literature indicates that aluminium already was successfully joined to magnesium by diffusion bonding with a pure nickel interlayer;[21] however, the strength of the welds was not reported. Nickel interlayer was also used with hybrid laser FSW technique where addition of nickel interlayer improved the strength due to the presence of more preferable Ni based intermetallic phases instead of Al–Mg compounds.[22]

The objective of the current study is to explore the effects of bare nickel and gold coated nickel interlayers on the microstructure and mechanical properties of the aluminium–magnesium resistance spot welds.

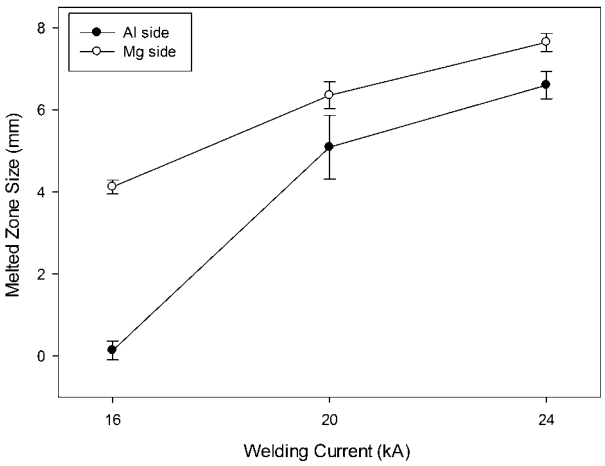

1 Correlation between melted zone size on both aluminium and magnesium side and welding current during RSW with bare nickel interlayer

Experimental

Welding specimens used in this study were commercially available sheets of magnesium alloy AZ-31B (3 wt-%Al and 1 wt-%Zn) and aluminium alloy 5754 (3 wt-%Mg, 0·5 wt-%Mn and 0·4 wt-%Fe). Pure nickel foil was used as the interlayer in this study, either in an uncoated condition or with an electrolytic gold plating typically 4–6 μm in thickness. Uncoated nickel used in this study was from an alternate supplier and slightly differs from the nickel used in our previous study,[24] where the interlayer in the present study has a more uniform hardness distribution through the thickness, and this led to some changes in the fracture location of the joints compared to prior work. Dimensions of the aluminium and magnesium alloy welding specimens were $100 \times 35 \times 2$ mm, while dimensions of the nickel based interlayers were $10 \times 10 \times 0{\cdot}2$ mm. The surface of the magnesium sheets was treated with solution of 2·5 g chromic oxide and 100 mL water before welding, and the aluminium coupons were ultrasonically cleaned in ethanol for 10 min and treated with solution of 1·2 mL HF, 67·5 mL HNO_3 and 100 mL water. Bare nickel interlayers were ultrasonically cleaned in acetone for 10 min, while gold coated nickel was used in as received condition.

The RSW equipment used in this study was a mid-frequency direct current resistance spot welder (built by Centerline Ltd), and the following welding parameters were employed: 4 kN electrode force, 16–24 kA welding current and a welding time of five cycles. Type FF-25 domed electrode caps made from a Cu–Cr–Zr alloy were used.

Three samples per condition were tested via tensile shear loading with welding currents of 16 and 20 kA, while six samples were tested with a welding current of 24 kA. An Instron 4206 (Norwood, MA, USA) tensile test machine was used in this study, where specimens were strained to failure with a crosshead speed of 1 mm min^{-1}. Alignment spacer sheets were used to grip the samples during overlap shear testing to minimise the bending or misalignment effects.

Metallographic weld specimens were cut, mounted, polished and examined by optical microscopy and scanning electron microscopy (SEM) equipped with energy dispersive X-ray analysis (EDX) using a JEOL JSM-6460. The size of the fusion nugget diameter was measured from the cross-sections on both the aluminium and magnesium side of the transverse weld sections, with a minimum of three samples per condition for nugget size measurement. Nital solution was used for etching of the magnesium alloy, while the aluminium alloy was etched with 2%HF. The fracture surface of the samples was examined by SEM and X-ray diffraction (XRD) techniques after tensile shear testing.

Results and discussion

Bare Ni interlayer

Weld geometry

No joints were produced with bare nickel interlayer in all range of currents from 16 to 24 kA. It was noted that when welding currents of 20 and 24 kA were employed, the aluminium sheet always separated from the nickel interlayer, suggesting that some bonding occurred between magnesium and the bare nickel interlayer.

Figure 1 shows the relationship between melted zone size and welding current. The bulk of the nickel interlayer remained solid with only partial melting of the surface during the welding, and therefore, aluminium and magnesium melted zone was measured separately. The melted zone size of the both sides increased with welding current as typically observed in RSW. It was noted that the magnesium alloy sheet had a larger melted zone than that observed in the aluminium alloy side in all conditions examined. Since more heat will be generated at the interface with higher contact resistance, this difference in the melted zone sizes may be explained by this variation. In general, contact resistance follows the volume resistivity of the metals involved.[25,26] Magnesium alloy AZ-31B has greater electrical resistivity (92 nΩ m) than aluminium alloy 5754 (49 nΩ m), which would lead to increased heat generation and larger melted zone in the magnesium sheet.[27,28] In addition, greater heat losses will be expected in the aluminium sheet due to the higher thermal conductivity of aluminium 5754 alloy (which is 147 W m^{-1} K^{-1}) compared to magnesium AZ-31B alloy (reported to be 96 W m^{-1} K^{-1}).[27,28]

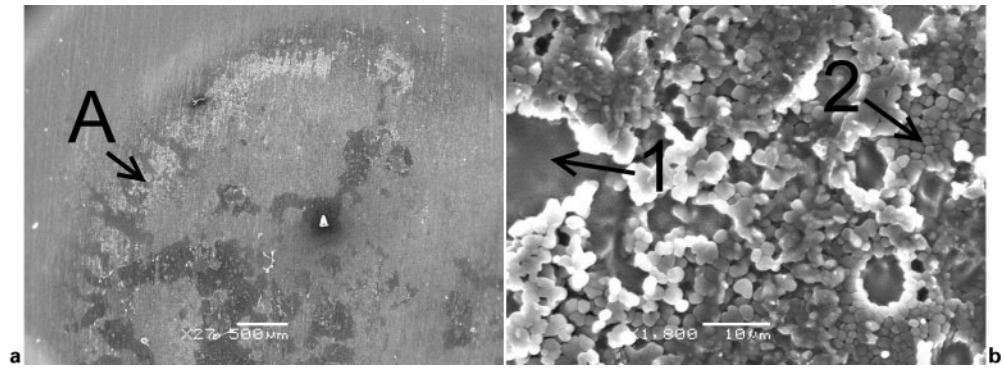

a overview; *b* details of region A in *a*

2 Fracture surface of bare nickel interlayer at aluminium side (with 24 kA)

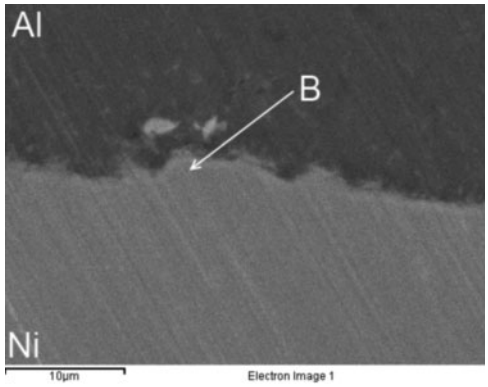

3 Image (SEM) of interface in aluminium–nickel weld (without magnesium)

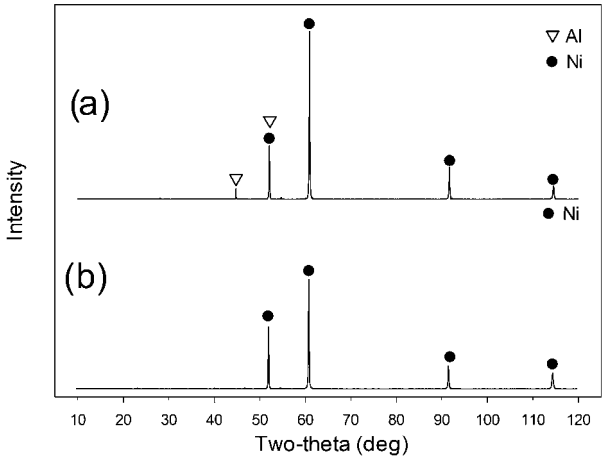

a aluminium side; *b* magnesium side

4 X-ray diffraction analysis of bare nickel interlayer fracture surface on both aluminium and magnesium side

Fracture surface

The fracture surface morphology was analysed on the sample made with 24 kA welding current. Figure 2 shows the fracture surface of the bare nickel interlayer at aluminium side. The results of EDX analysis of the different areas shown in Fig. 2 are summarised in Table 1. The evidence of molten aluminium, which resolidified on the surface of the nickel interlayer, can only be observed in a narrow semicircle area at the periphery of the nugget (region A in Fig. 2*a*). At this region, aluminium grains and dendrites (region 2 in Fig. 2*b*) are observed growing from the nickel surface (region 1 in Fig. 2*b*), and it appears that this region did not contribute to the strength.

The absence of significant metallurgical reaction between aluminium and nickel is in contrast with RSW of aluminium to nickel without magnesium sheet. It was found that aluminium and nickel sheets employed in this study can be successfully spot welded and then magnesium sheet is not present. In this case, the bulk of the nickel interlayer was not melted, while the aluminium sheet did, similar to the welding of aluminium to magnesium with a bare nickel interlayer. However, reaction between aluminium and nickel can be observed along aluminium fusion zone/nickel interface when no magnesium sheet was present. Figure 3 shows the SEM image of the aluminium/nickel interface of a weld made without a magnesium sheet. The composition of the reaction layer marked as B on Fig. 3 is 65·1 wt-%Ni and 34·9 wt-%Al, indicating that metallurgical bonding is possible between aluminium and nickel when only the two sheets are used. These observations suggest that more heat was generated in the nickel sheet compared to when the magnesium sheet was present, since all the other conditions were kept the same. The poor bonding observed in Fig. 2 may be a result of lower heat generation caused by the spreading of the current, which has a tendency to occur during RSW of three sheet aluminium assemblies.[25]

Table 1 Energy dispersive X-ray analysis quantification of different areas in Fig. 2b/wt-%

Area	Mg	Al	Ni
1	…	25·2	74·8
2	3·0	92·4	4·6

The nickel interlayer stayed attached to the magnesium surface, which suggests that some wetting and/or reaction between magnesium and nickel occurred. A similar phenomenon was observed during diffusion bonding of aluminium to magnesium with nickel interlayer,[21] where reaction at magnesium/nickel interface started much earlier than at aluminium/nickel interface.

X-ray diffraction analysis was carried out on the fracture surface of bare nickel interlayer on both aluminium and magnesium side (Fig. 4). The sample made with 24 kA welding current was used for the analysis. Aluminium sheet was separated from nickel interlayer without applying any force, while magnesium sheet was forced to separate from nickel. No intermetallic compounds were detected on the nickel surface on both aluminium and magnesium side using XRD. Although Al–Ni phases were

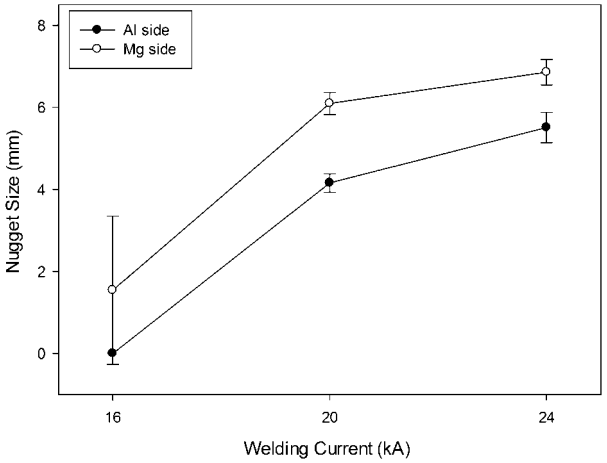

5 Correlation between nugget size on both aluminium and magnesium side and welding current during RSW with gold coated nickel interlayer

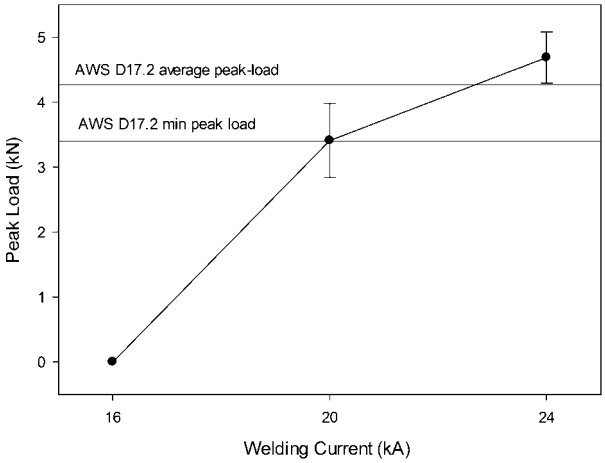

6 Correlation between peak load and welding current during RSW of aluminium to magnesium with gold coated nickel interlayer

detected by EDX (Table 1), the small amount and fine thickness of those phases was beyond the resolution of XRD, making it hard to be observed.

Welds made with gold coated nickel interlayer

Tensile shear test and weld geometry

Since no joints occurred during RSW of aluminium to magnesium with bare nickel interlayer due to low heat generation in the nickel sheet, it was concluded that addition of very thin layer of a good braze material with melting point lower than that of nickel likely will improve metallurgical reaction at the aluminium/nickel and magnesium/nickel interfaces. Gold is known as a good braze metal, and it is commonly used as plating in microelectronics soldering. The literature also indicates that even solid state bonds of gold coated nickel sheets might be stronger than the bare nickel joints with a fusion nugget.[29] Therefore, in order to improve metallurgical boding and mechanical performance of aluminium–magnesium dissimilar joints, experiments with gold coated nickel were conducted. The same welding parameters as for bare nickel interlayer were used.

The relationship between nugget size and welding current is shown in Fig. 5. The nugget dimensions on the magnesium side were always larger than those of the aluminium side as in the case when a bare nickel interlayer was used (Fig. 1). It was also noted that nuggets on both aluminium and magnesium side were smaller than in the case with a bare nickel interlayer. Based on the samples made with 24 kA welding current, the nugget on aluminium side was on average 1·1 mm smaller, while the nugget on magnesium side was about 0·8 mm smaller than those obtained with a bare nickel interlayer. This decrease in nugget size was caused by the lack of an oxide on the gold surface and therefore lower contact resistance and heat generation at both aluminium/nickel and magnesium/nickel interfaces.

Figure 6 shows influence of welding current on peak load during tensile shear test. It can be seen that fracture loads increased with welding current. No joints were achieved with 16 kA welding current because insufficient amount of heat was generated, and joints were produced when the welding current increased to 20 or 24 kA. During tensile shear testing, welds made with 24 kA welding current, which was the optimal condition in the study, always failed at the magnesium/nickel interface, suggesting that the aluminium/nickel interface was stronger.

Welds made with 24 kA had average peak load of 4·69 kN with a minimum of 4·34 kN, while requirement of the AWS D17·2 standard is average of 4·27 kN with a minimum of 3·4 kN; hence, the welds easily met requirement of the standard based on the ultimate strengths and sheet thickness of the base materials.[30] Furthermore, the average fracture load was as high as 90% of the strength of same size optimised AZ-31B similar joints.[31,32] Recently, Patel *et al.*[18] made an attempt to compare lap shear strengths of aluminium–magnesium dissimilar spot welds made by different welding techniques based on the data from the studies currently available in the literature. The highest strength achieved was reported as 42 MPa by using an ultrasonic spot welding technique with a tin interlayer.[18] Following the same calculation steps as employed by Patel *et al.*, the lap shear strength of the welds achieved in the current study would reach 127 MPa. However, as was mentioned by Patel *et al.*, there was difference between studies in the thickness of the samples and in the types of aluminium and magnesium alloys. In addition, the nugget diameter for RSW and shoulder diameter for FSSW were used to calculate the respective areas for determination of lap shear strength, which is not directly comparable.

Interfacial microstructure

Interfacial microstructure analysis was conducted on the samples made with 24 kA welding current. Figure 7 shows typical interfacial microstructure of aluminium–magnesium joint made with gold coated nickel interlayer. There are much more interfacial defects such as voids and

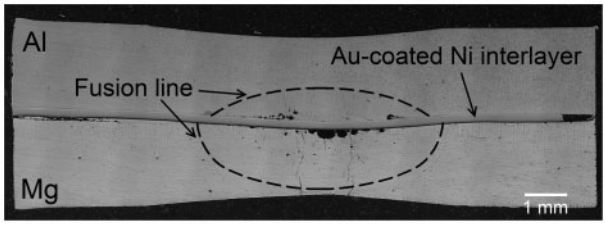

7 Typical aluminium–magnesium weld made with gold coated nickel interlayer (with 24 kA)

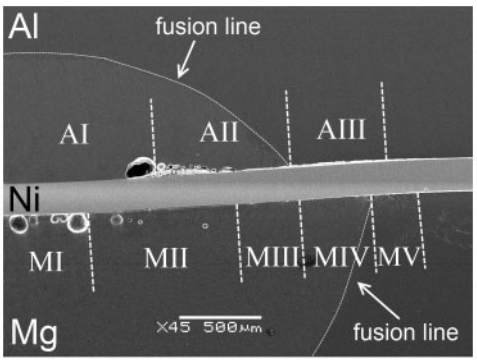

8 Location of zones that exhibit different interfacial microstructure in aluminium/magnesium weld made with gold coated nickel interlayer (with 24 kA)

pores at the magnesium/nickel interface than at the aluminium/nickel interface. It was also noted that pores and cracks at magnesium/nickel interface mostly concentrated in the centre of a nugget, which is typical for RSW of magnesium alloys.[33,34] The average pore size observed at magnesium/nickel interface was close to 75 µm. Porosity is a common defect in RSW of magnesium alloys. Evaporation of magnesium and hydrogen absorption are the primary mechanisms that lead to formation of the porosity.[31,35] Some cracks are also observed in aluminium and magnesium fusion zones, which is not unexpected, since solidification cracks are very common in RSW of both aluminium and magnesium alloys.[36–38] The details of the interfacial microstructure of both interfaces are analysed in the following subsections.

Aluminium/nickel interface

There are three distinct zones in the aluminium/nickel interface such as shown in Fig. 8. The centre of the nugget was denoted as zone AI, the edge of a nugget as zone AII and the region adjunct to the nugget as zone AIII. Details of the zone AI are shown in Fig. 9*a*. None of the gold coating can be found between aluminium and nickel in this zone (spectrum 3 in Table 2). As evident in Fig. 9*a*, gold material was clearly dissolving into the bulk aluminium fusion zone and segregated along dendrite and grain boundaries (region 4 in Fig. 9*a*). The microstructure of zones AII and AIII is shown in Figs. 9*b* and *c*. In zones AII and AIII, aluminium was joined to the nickel by a gold rich layer, which acted as a filler metal. The microstructure of this gold rich filler metal is shown in Fig. 9*d*, where the composition of this layer was roughly the same in both zones AII and AIII—21·3 wt-%Al and 78·7 wt-%Au. Microstructure and composition of this layer suggest that it was gold coating alloyed with aluminium. The only difference between zones AII and AIII is that zone AII is located inside the fusion zone and zone AIII is just beyond the fusion line. As can be seen in Fig. 8, the thickness of the gold rich layer is increasing from zone AII to the middle of zone AIII, which suggests that displacement of the gold rich layer towards the outer diameter of the interface between aluminium and nickel occurred. The displacement of the gold rich layer led to the formation of the direct contact between aluminium fusion zone and bare nickel surface in the centre of a nugget (zone AI). In addition, higher temperatures at

Table 2 Energy dispersive X-ray analysis quantification of different areas in Fig. 9/wt-%

Spectrum	Mg	Al	Ni	Au
3	…	20·6	79·4	…
4	3·8	82·4	…	13·8

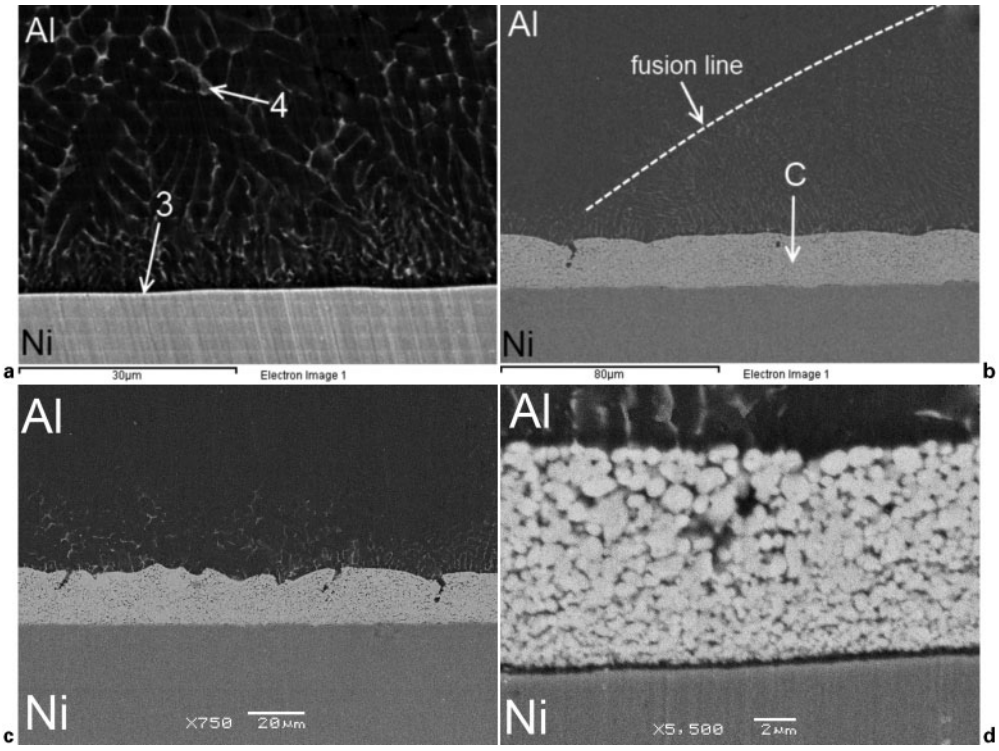

a zone AI; *b* zone AII; *c* zone AIII; *d* details of region C from *b*

9 Aluminium/nickel interface of weld (with Au coated Ni interlayer, 24 kA), which corresponds to interfaces noted in Fig. 8

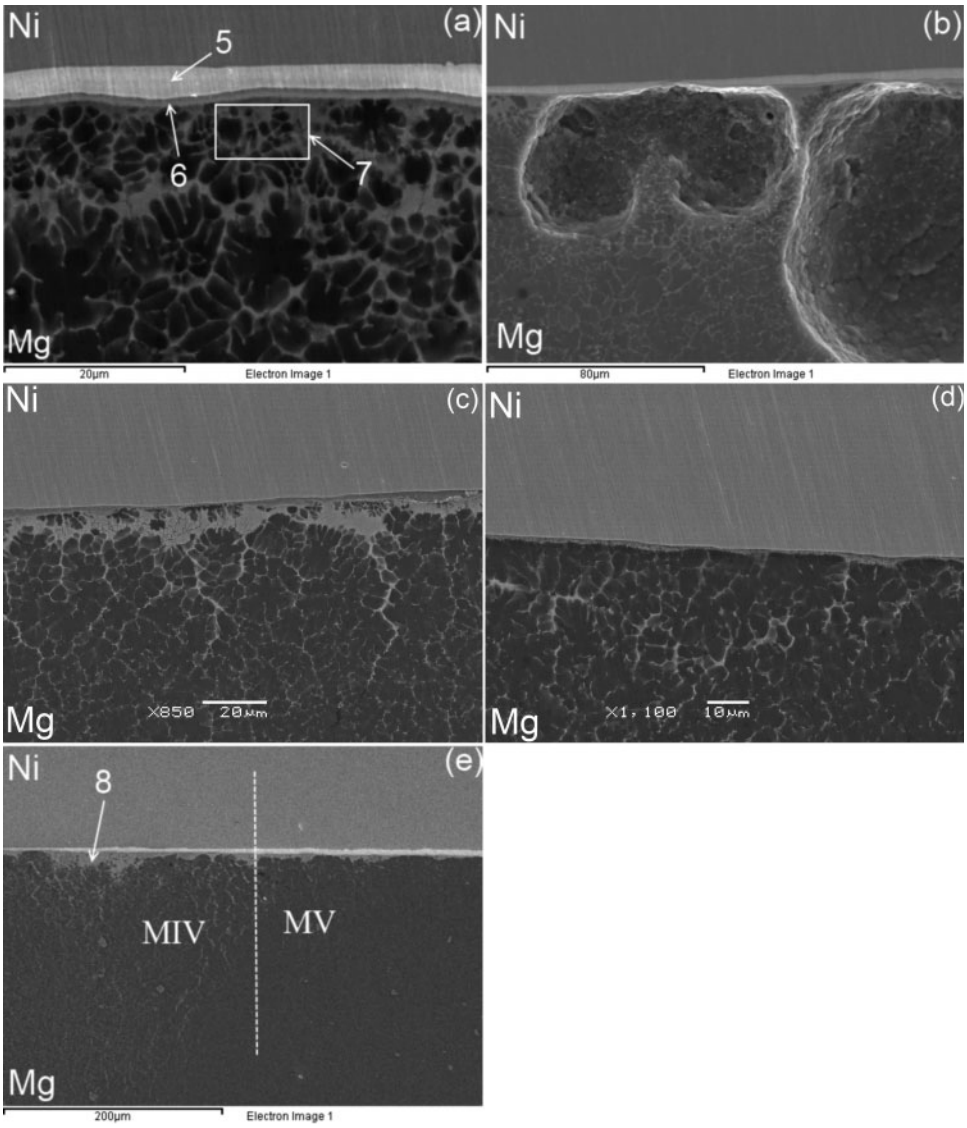

a, *b* zone MI; *c* zone MII; *d* zone MIII; *e* zones MIV and MV

10 Magnesium/nickel interfaces in weld (with Au coated Ni interlayer, 24 kA), which corresponds to interfaces noted in Fig. 8

the centre of a nugget likely led to more intensive distribution of gold into the aluminium fusion zone in this region, which might have contributed to the depletion of gold coating in the centre.

Magnesium/nickel interface

Interfacial microstructure of the magnesium/nickel interface is more complex than that of aluminium/nickel interface. Five distinct zones with different microstructure features can be observed at magnesium/nickel interface. The zones were named MI, MII, MIII, MIV and MV from the centre to the edge of a nugget respectively (Fig. 8).

The microstructure of zone MI is shown in Fig. 10*a* and *b*. Gold was distributing into magnesium fusion zone, in a similar manner to aluminium/nickel interface in the centre (Fig. 9*a*). However, unlike in the centre of aluminium/nickel interface, magnesium was not joined to the nickel directly. There are two different continuous and smooth gold rich layers between magnesium and nickel in zone MI (regions 5 and 6 in Fig. 10*a*). Based on the EDX results (Table 3), the lighter layer (region 5 in Fig. 10*a*) is the remnant of the original gold coating, while a darker and thinner gold rich layer (region 6 in Fig. 10*a*) is Mg_3Au intermetallic compound.[39] The formation of monolithic layer of Mg_3Au intermetallic suppressed further distribution of gold coating into magnesium fusion zone, and therefore, significant amount of original gold coating remained undisturbed (region 5 in Fig. 10*a*). Away from the continuous layer of Mg_3Au compound is magnesium fusion zone, which was heavily enriched in gold (region 7 in Fig. 10*a*). Based on the gold–magnesium phase diagram (Fig. 11),[39] this region is likely gold–magnesium eutectic structure, which consists of Mg_3Au intermetallic compound and α-magnesium. Numerous voids can also be found in zone MI (Fig. 10*b*). The voids were formed on the surface of the continuous Mg_3Au layer and likely slowed the diffusion of gold into magnesium fusion zone.

Table 3 Energy dispersive X-ray analysis quantification of different areas in Fig. 10/wt-%

Spectrum	Mg	Al	Ni	Au
5	1·2	…	3·8	95·0
6	24·9	…	2·3	72·8
7	57·8	2·0	…	40·2

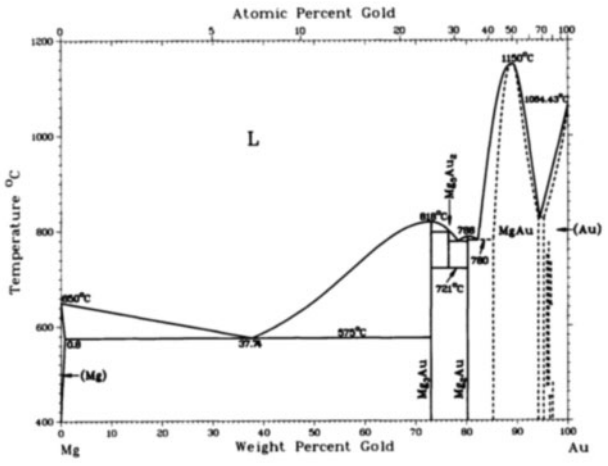

11 Gold–magnesium binary phase diagram[39]

In contrast with zone MI, no remnant of the original gold coating (region 5 in Fig. 10*a*) and no continuous Mg_3Au layer (region 6 in Fig. 10*a*) can be observed in zone MII (Fig. 10*c*). Temperatures in this region were likely lower than in zone MI, and therefore, the Mg_3Au compound did not form as continuous smooth layer, leading to the more extensive diffusion of gold into magnesium fusion zone. The absence of the interfacial defects also likely contributed to the intensive migration of gold into magnesium. Gold–magnesium eutectic structure similar to that in zone MI (region 7 in Fig. 10*a*) is still present at the interface, indicating that molten magnesium comes into little direct contact with nickel surface at the region.

The microstructure of zone MIII is shown in Figs. 8 and 10*d*. It is similar to the zone MII; however, there is much less gold in the magnesium fusion zone near nickel surface and molten magnesium contacts bare nickel surface in many locations.

Microstructures observed in zones MIV and MV are shown in Fig. 10*e*. The remaining original gold coating appears in the beginning of zone MIV, and its thickness increases approaching the nugget edge. The microstructure of zone MIV is similar to that of zone MI; however, no defects can be observed in this region, and it was not determined whether Mg_3Au formed as a continuous layer as observed in zone MI (region 6 in Fig. 10*a*). The amount of magnesium fusion zone heavily enriched in gold in zone MIV (region 8 in Fig. 10*e*) is much larger than that in zone MIII, which suggests that squeezing of this phase from zone MIII to zone MIV may have occurred. The microstructure of zone MV is similar to that of zone MIV; however, it is located beyond the fusion line. Surface melting of gold and partial melting of magnesium likely occurred in zone MV, leading to microstructures similar to zone MIV.

Fracture surface analysis

Fracture surface morphology was analysed on the samples made with 24 kA welding current. All the samples made with this conditions failed at magnesium/nickel interface during the tensile shear test. The gold coated nickel interlayer was separated from aluminium sheet after the tensile shear test in order to analyse fracture surface at aluminium side. Fracture surfaces at the aluminium and magnesium sides were analysed separately, and details of the analysis were summarised in the following subsections.

Aluminium/nickel interface

Fracture surface of the gold coated nickel interlayer at aluminium side is shown in Fig. 12. Regions of the fracture

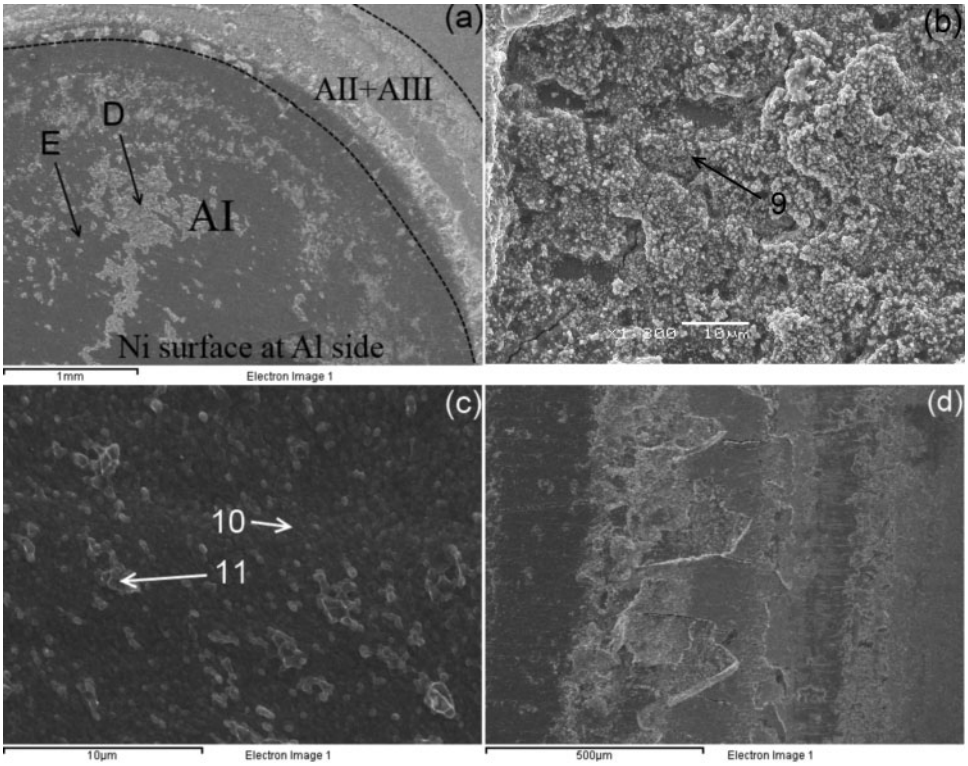

a overview; *b* zone D from *a*; *c* details of zone E from *a*; *d* details of zone AII + AIII from *a*

12 Fracture surface of gold coated nickel interlayer at aluminium side (with 24 kA)

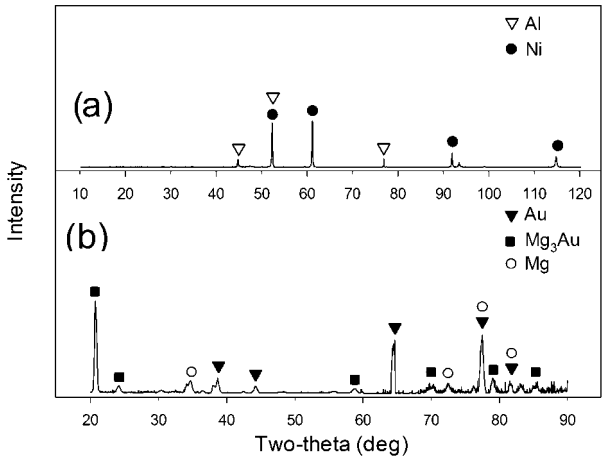

a aluminium side; *b* magnesium side

13 X-ray diffraction analysis of gold coated nickel interlayer fracture surface on both aluminium and magnesium side

surface that correspond to the interfacial microstructure zones AI, AII and AIII (Fig. 8) are shown in Fig. 12*a*.

Two regions with different morphologies and compositions can be found in zone AI, the regions marked as D and E in Fig. 12*a*. The composition (spectrum 9 in Table 4) and morphology of region D (Fig. 12*b*) suggest that in this region, failure occurred within the aluminium fusion zone enriched in gold. Meanwhile, in region E, failure occurred at molten aluminium/nickel interface, since the region exhibits bare nickel surface (region 10 in Fig. 12*c*) with only small amount of aluminium rich particles attached to it (region 11 in Fig. 12*c*).

The chemical composition of the fracture surface in zones AII and AIII is 90·8 wt-%Au and 9·2 wt-%Al, which suggests that failure in this region occurred inside gold rich phase, which acted as a filler metal between aluminium and nickel (Fig. 9*d*).

Comparing these observations to the fracture morphology analysis of the sample made with bare nickel interlayer (Fig. 2), it is clear that the addition of gold coating greatly improved metallurgical bonding at the aluminium/nickel interface. The major contribution of gold was that it acted as a filler metal at the edge of a nugget and at the region adjunct to a nugget (zones AII and AIII). In addition, in the centre of a nugget zone (AI), failure partially occurred through aluminium fusion zone, which suggests that this region also contributed to the strength. This can be explained by the fact that nickel surface was completely clean and oxide free under the gold coating, which promoted better wetting and bonding at the region. The same role played zinc coating during RSW of magnesium to steel, where zinc was melted and squeezed to the periphery, leaving clean steel surface for bonding at the centre and acting as a filler metal at the periphery, which led to the formation of higher strength welds.

Table 4 Energy dispersive X-ray analysis quantification of different areas in Fig. 12/wt-%

Spectrum	Al	Ni	Au
9	49·2	7·3	43·5
10	…	96·8	3·2
11	83·5	12·3	4·2

X-ray diffraction analysis of the fracture surface of the gold coated nickel interlayer on aluminium side did not detect any Al–Ni intermetallics (Fig. 13*a*). Similarly to the case with a bare nickel interlayer, possible Al–Ni intermetallics were detected by EDX (Table 4); however, the size and amount of these phases were beyond the resolution of XRD.

Magnesium/nickel interface

Figure 14 shows fracture surface morphology of the gold coated nickel interlayer at magnesium side. Regions of the fracture surface that correspond to the interfacial microstructure zones MI–MV (Fig. 8) are shown in Fig. 14*a*.

The morphology (Fig. 14*b*) and chemical composition (Table 5) of zone MI suggest that failure in this region occurred inside magnesium fusion zone very close to continuous Mg_3Au layer (Fig. 10*a*), except locations where pores and voids were observed. Flat surface of the Mg_3Au intermetallic layer can be found (region 13 in Fig. 14*b*) under the voids (Fig. 10*b*).

The fracture surface of zone MII exhibits a ductile morphology. The chemical composition of the region suggests that failure in this region occurred inside the magnesium fusion zone at significant distance from the interface, since amount of gold in this region (spectrum 14 in Table 5) is much lower than in magnesium fusion zone near the interface.

The fracture morphology of zone MIII exhibits bare nickel surface (region 15 in Fig. 14*d*) with magnesium material only occasionally attached to it (region 16 in Fig. 14*d*). This suggests that bare nickel surface accommodated less molten magnesium material than zones MI and MII where gold rich phases existed between the nickel surface and bulk of the magnesium fusion zone.

Zones MIV and MV produced similar fracture morphologies. The composition and morphology of regions marked as MIV and MV on Fig. 14*a* suggest that failure occurred along the surface of the residual gold coating, which was partially melted (region 17 in Fig. 14*e*).

X-ray diffraction analysis, which was carried out on the fracture surfaces of the gold coated nickel interlayer at magnesium side, indicated the presence of Mg_3Au intermetallic compound (Fig. 13*b*), which supports the findings made regarding the interfacial microstructure and fracture surfaces using SEM and EDX techniques.

Conclusions

Mechanical and microstructural properties of the dissimilar aluminium–magnesium resistance spot welds with bare and gold coated nickel interlayers are investigated in this study.

No joints were produced using a bare nickel interlayer. Limited bonding between magnesium and bare nickel interlayer still occurred, since they did not separate right after the welding. In order to improve metallurgical bonding, experiments with gold coated nickel interlayer were conducted and this produced much higher strength aluminium–magnesium resistance spot welds. The welds produced with welding current of 24 kA had average peak load of 4·69 kN, which was as high as 90% of the optimised similar AZ-31B welds. The welds made with 24 kA welding current also easily passed requirements of

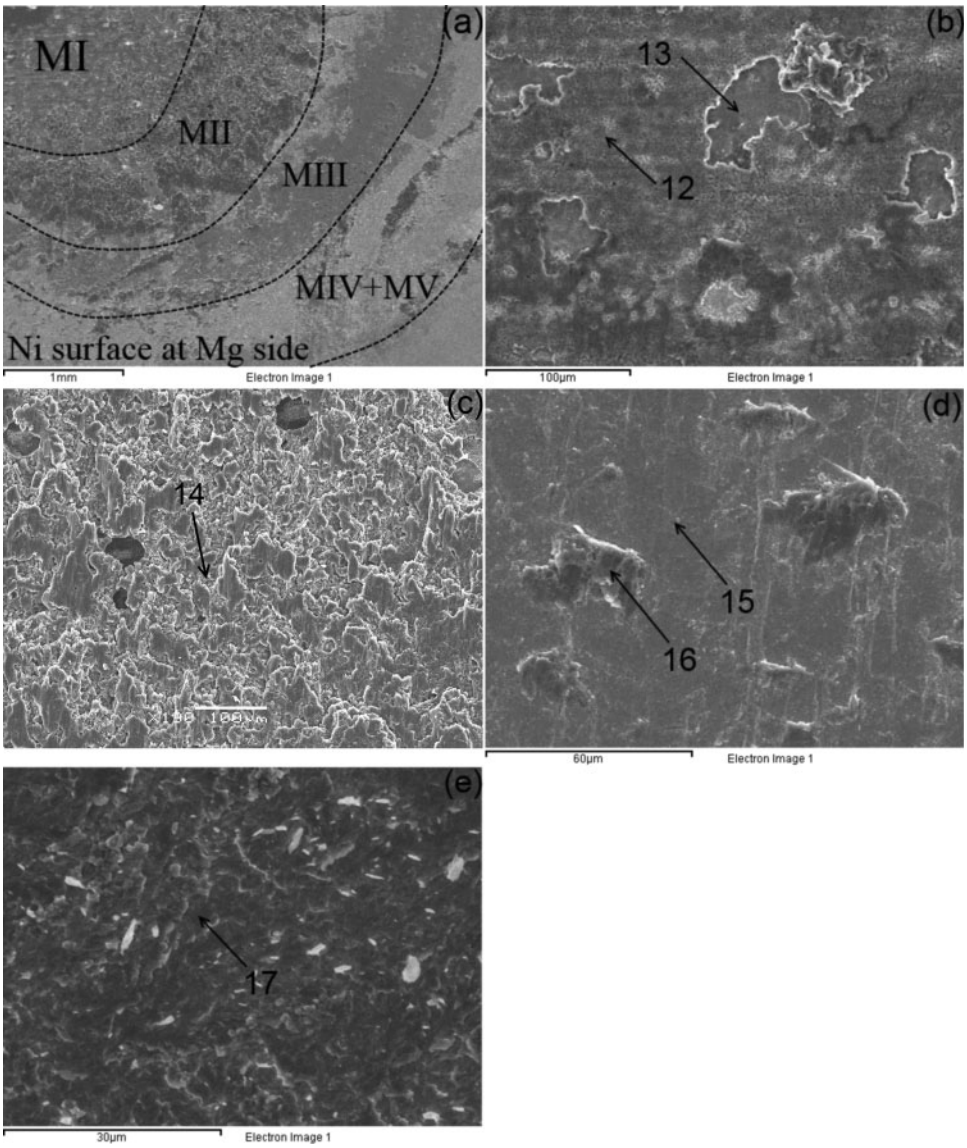

a overview; *b* details of zone MI from *a*; *c* details of zone MII from *a*; *d* details of zone MIII from *a*; e details of zones MIV and MV from *a*

14 Fracture surface of gold coated nickel interlayer at magnesium side (with 24 kA)

AWS D17·2 standard (4·27 kN). The formation of Al–Mg intermetallic compounds was completely suppressed using a gold coated nickel interlayer. This is a result of the fact that the interlayer remained intact during the welding due to its high melting point compared to aluminium and magnesium. The addition of gold significantly contributed to the metallurgical bonding of the sheets, resulting in higher weld strength. Aluminium was joined to nickel by direct welding brazing in the centre and by brazing through gold based filler metal at the edges of a nugget and at the adjunct to the nugget region. Magnesium was joined to nickel mostly through different gold rich phases, such as residual gold coating, Mg_3Au intermetallic compound layer and gold–magnesium eutectic structure. Employing an interlayer with high melting point coated with good brazing material, such as gold coated nickel, clearly represents a promising approach in dissimilar resistance spot welding.

Table 5 Energy dispersive X-ray analysis quantification of different areas in Fig. 14/wt-%

Spectrum	Mg	Ni	Au
12	55·0	…	45·0
13	24·3	…	75·7
14	82·3	…	17·7
15	…	100·0	…
16	79·6	20·4	…
17	6·7	…	93·3

References

1. N. Jeal: *Adv. Mater. Process.*, 2005, **163**, (9), 65–67.
2. R. Borrisutthekul, Y. Miyashita and Y. Mutoh: *Sci. Technol. Adv. Mater.*, 2005, **6**, (2), 199–204.
3. L. Liu and H. Wang: *Metall. Mater. Trans. A*, 2011, **42A**, (4), 1044–1050.
4. F. Hayat: *Mater. Des.*, 2011, **32**, 2476–2484.
5. P. Liu, Y. Li, H. Geng and J. Wang: *Mater. Lett.*, 2007, **61**, (6), 1288–1291.
6. G. Mahendran, V. Balasubramanian and T. Senthilvelan: *Mater. Des.*, 2009, **30**, (4), 1240–1244.
7. Y. Li, P. Liu, J. Wang and H. Ma: *Vacuum*, 2007, **82**, (1), 15–19.

8. Y. Chen and K. Nakata: *Scr. Mater.*, 2008, **58**, (6), 433–436.
9. Y. S. Sato, S. H. C. Park, M. Michiuchi and H. Kokawa: *Scr. Mater.*, 2004, **50**, 1233–1236.
10. A. Somasekharan and L. Murr: *Mater. Charact.*, 2004, **52**, (1), 49–64.
11. Y. Sato, A. Shiota, H. Kokawa, K. Okamoto, Q. Yang and C. Kim: *Sci. Technol. Weld. Join.*, 2010, **15**, (4), 319–324.
12. A. Kostka, R. Coelho, J. Dos Santos and A. Pyzalla: *Scr. Mater.*, 2009, **60**, (11), 953–956.
13. A. Panteli, J. Robson, I. Brough and P. Prangnell: *Mater. Sci. Eng. A*, 2012, **A556**, 31–42.
14. V. Patel, S. Bhole and D. Chen: *Sci. Technol. Weld. Join.*, 2012, **17**, (3), 202–206.
15. L. Zhao and Z. Zhang: *Scr. Mater.*, 2008, **58**, (4), 283–286.
16. L. Liu, X. Liu and S. Liu: *Scr. Mater.*, 2006, **55**, 383–386.
17. Y. Wang, G. Luo, J. Zhang, Q. Shen and L. Zhang: *Mater. Sci. Eng. A*, 2013, **A559**, 868–874.
18. V. K. Patel, S. D. Bhole and D. L. Chen: *Sci. Technol. Weld. Join.*, 2012, **17**, (5), 342–347.
19. M. Gao, S. Mei, X. Li and X. Zeng: *Scr. Mater.*, 2012, **67**, 193–196.
20. J. Shang, K. Wang, Q. Zhou, D. Zhang, J. Huang and G. Li: *Mater. Des.*, 2012, **34**, 559–565.
21. J. Zhang, G. Luo, Y. Wang, Q. Shen and L. Zhang: *Mater. Lett.*, 2012, **83**, 189–191.
22. W.-S. Chang, S. Rajesh, C.-K. Chun and H.-J. Kim: *J. Mater. Sci. Technol.*, 2011, **27**, (3), 199–204.
23. D. Shi, B. Wen, R. Melnik, S. Yao and T. Li: *J. Solid State Chem.*, 2009, **182**, (10), 2664–2669.
24. P. Penner, L. Liu, A. Gerlich and Y. Zhou: 'Effects of Au coated Ni interlayer on dissimilar resistance spot welding of Al to Mg', Proc. Sheet Metal Welding Conf. XV, Livonia, MI, USA, October 2012, American Welding Society (Detroit Section), 4–4.
25. RWM Association: 'Resistance welding manual', 4th edn; 2003, Philadelphia, PA, RWMA.
26. W. Tan, S. Lawson and Y. Zhou: *Metall. Mater. Trans. A*, 2005, **36A**, (7), 1901–1910.
27. Aalco: 'Aluminium alloys – Aluminium 5754 properties, fabrication and applications, supplier data by Aalco', 2011. http://www.azom.com/article.aspx?ArticleID=2806
28. ASM International: 'Properties & selection – Nonferrous alloys & special-purpose materials'; 1990, Metals Park, OH, ASM International.
29. W. Tan, Y. Zhou and H. Kerr: *Metall. Mater. Trans. A*, 2002, **33A**, (8), 2667–2676.
30. American Welding Society: 'D 17·2/D17·2M:2013 – specification for resistance welding for aerospace applications'; 2007, Miami, FL, American Welding Society.
31. L. Liu, S. Zhou, Y. Tian, J. Feng, J. Jung and Y. Zhou: *Sci. Technol. Weld. Join.*, 2009, **14**, (4), 356–361.
32. L. Liu, L. Xiao, J. C. Feng, Y. H. Tian, S. Q. Zhou and Y. Zhou: *Metall. Mater. Trans. A*, 2010, **41A**, 2642–2650.
33. L. Liu, L. Xiao, J. Feng, Y. Tian, S. Zhou and Y. Zhou: *Metall. Mater. Trans. A*, 2010, **41A**, (10), 2651–2661.
34. R. Qiu, H. Shi, H. Yu, K. Zhang, Y. Tu and S. Satonaka: *Mater. Manuf. Processes*, 2010, **25**, (11), 1304–1308.
35. H. Zhao and T. DebRoy: *Weld. J.*, 2001, **80**, (8), 204–210.
36. R. Florea, D. Bammann, A. Yeldell, K. Solanki and Y. Hammi: *Mater. Des.*, 2013, **45**, 456–465.
37. D. Sun, B. Lang, D. Sun and J. Li: *Mater. Sci. Eng. A*, 2007, **A460**, 494–498.
38. N. K. Babu, S. Brauser, M. Rethmeier and C. Cross: *Mater. Sci. Eng. A*, 2012, **A549**, 149–156.
39. ASM International: 'Alloy phase diagrams'; 1992, Metals Park, OH, ASM International.